

# UCSF

## UC San Francisco Previously Published Works

### Title

The clustered gamma protocadherin Pcdh $\gamma$ C4 isoform regulates cortical interneuron programmed cell death in the mouse cortex.

### Permalink

<https://escholarship.org/uc/item/0jr6z39c>

### Journal

Proceedings of the National Academy of Sciences of USA, 121(6)

### Authors

Leon, Walter  
Steffen, David  
Dale-Huang, Fiona  
et al.

### Publication Date

2024-02-06




### DOI

10.1073/pnas.2313596120

Peer reviewed



# The clustered gamma protocadherin *Pcdh $\gamma$ C4* isoform regulates cortical interneuron programmed cell death in the mouse cortex

Walter R. Mancia Leon<sup>a,1</sup>, David M. Steffen<sup>ab,1</sup> , Fiona R. Dale-Huang<sup>a</sup>, Benjamin Rakela<sup>c</sup>, Arnar Breevoort<sup>c</sup>, Ricardo Romero-Rodriguez<sup>a</sup>, Andrea R. Hasenstaub<sup>d,e</sup>, Michael P. Stryker<sup>c,e</sup> , Joshua A. Weiner<sup>b</sup>, and Arturo Alvarez-Buylla<sup>a,e,2</sup> 

Contributed by Arturo Alvarez-Buylla; received August 7, 2023; accepted November 16, 2023; reviewed by Natalia V. De Marco Garcia and Gordon Fishell

Cortical inhibitory interneurons (cINs) are born in the ventral forebrain and migrate into the cortex where they make connections with locally produced excitatory glutamatergic neurons. Cortical function critically depends on the number of cINs, which is also key to establishing the appropriate inhibitory/excitatory balance. The final number of cINs is determined during a postnatal period of programmed cell death (PCD) when ~40% of the young cINs are eliminated. Previous work shows that the loss of clustered gamma protocadherins (*Pcdhgs*), but not of genes in the *Pcdha* or *Pcdhb* clusters, dramatically increased BAX-dependent cIN PCD. Here, we show that *Pcdh $\gamma$ C4* is highly expressed in cINs of the mouse cortex and that this expression increases during PCD. The sole deletion of the *Pcdh $\gamma$ C4* isoform, but not of the other 21 isoforms in the *Pcdhg* gene cluster, increased cIN PCD. Viral expression of the *Pcdh $\gamma$ C4*, in cIN lacking the function of the entire *Pcdhg* cluster, rescued most of these cells from cell death. We conclude that *Pcdh $\gamma$ C4* plays a critical role in regulating the survival of cINs during their normal period of PCD. This highlights how a single isoform of the *Pcdhg* cluster, which has been linked to human neurodevelopmental disorders, is essential to adjust cIN cell numbers during cortical development.

GABAergic | neuronal elimination | inhibitory neurons | medial ganglionic eminence | transplantation

Programmed cell death (PCD) is a key feature of the development of the nervous system essential to adjust the size of neuronal cell populations (1). The mechanisms of how neuronal numbers are adjusted are largely based on studies of the peripheral nervous system (PNS), where neuronal cell death is largely explained by the neurotrophic factor hypothesis (2–7). However, the mechanism determining the size of a neuronal population in the central nervous system (CNS) and how PCD is controlled remains largely unknown. Several studies indicate that the CNS does not utilize the neurotrophic-related molecular mechanisms used in the PNS to regulate PCD (8–11).

In the cerebral cortex, local circuit inhibitory neurons, or cortical inhibitory interneurons (cINs), are essential for sculpting, gating, and regulating neuronal excitation. Dysfunction or changes in the number of cINs is a hallmark of neurological disorders including epilepsy, schizophrenia, and autism (12–17). Ensuring the proper number of cINs during cerebral cortex development is an essential step in establishing proper brain function.

cINs are produced in the ventral forebrain within the medial and caudal ganglionic eminences (MGE and CGE). The young cINs then migrate dorsally into the cortex and form connections with locally produced excitatory neurons. Within the first two postnatal weeks of cortical development in mice, approximately 40% of cINs are eliminated by PCD (11, 18). An intriguing feature of this developmental process of cell elimination is its timing and location. While most cINs are born in the ventral telencephalon between E11.5 and 16.5, their PCD occurs postnatally, 10 to 15 d later, and in the cortex, far from their birthplace. The timing of cIN PCD correlates with several features of cortical development including the emergence of correlated activity and the development of cIN morphological complexity and synaptic connectivity (19–24). Indeed, changes in correlated neuronal activity during the timing of PCD have been associated with altered cIN survival (25). Adhesion proteins are likely necessary to establish the initial cell–cell connectivity that is key to the regulation of PCD in the cortex.

The clustered protocadherins (*Pcdhs*) (26) are a set of 58 cell surface homophilic-adhesion molecules that are tandemly arranged in three subclusters named alpha, beta, and gamma: *Pcdha*, *Pcdhb*, and *Pcdhg* (27). *Pcdhs* play important roles in neuronal tiling, dendritic arborization, and axon targeting (28–32). Loss of function of the 22 *Pcdhg* isoforms, but not of the *Pcdha* or *Pcdhb* gene clusters, results in increased BAX-dependent interneuron cell death in the cortex, spinal cord, and retina (33–35). Using transplantation to bypass neonatal lethality, we have also shown that the combined removal of three *Pcdhy* isoforms (*PcdhyC3*, *PcdhyC4*, and *PcdhyC5*) resulted in increased cIN cell death. Importantly, the

## Significance

During cortical development, inhibitory neuron numbers are refined during a process of programmed cell death (PCD) which is critical for the excitatory/inhibitory balance required for proper brain function. In this paper, we show that the *Pcdh $\gamma$ C4* isoform of the  $\gamma$ -protocadherins was expressed in MGE-derived cortical interneurons during the period of programmed cell death. This isoform was both necessary and sufficient for normal neuronal elimination during the period of programmed cell death. These findings provide a key molecular component to understand the mechanisms through which individual interneurons survive and integrate into the cortical circuits or undergo PCD.

Author contributions: W.R.M.L., D.M.S., B.R., A.R.H., M.P.S., J.A.W., and A.A.-B. designed research; W.R.M.L., D.M.S., F.R.D.-H., R.R.-R., and A.A.-B. performed research; W.R.M.L., D.M.S., A.B., A.R.H., J.A.W., and A.A.-B. contributed new reagents/analytic tools; W.R.M.L., D.M.S., F.R.D.-H., B.R., R.R.-R., A.R.H., M.P.S., J.A.W., and A.A.-B. analyzed data; and W.R.M.L., D.M.S., B.R., A.R.H., M.P.S., J.A.W., and A.A.-B. wrote the paper.

Reviewers: N.V.D.M.G., Weill Cornell Medicine; and G.F., Harvard Medical School.

Competing interest statement: A.A.-B. is co-founder and advisor to Neurona Therapeutics and holds stocks in Neurona Therapeutics.

Copyright © 2024 the Author(s). Published by PNAS. This open access article is distributed under [Creative Commons Attribution-NonCommercial-NoDerivatives License 4.0 \(CC BY-NC-ND\)](https://creativecommons.org/licenses/by-nc-nd/4.0/).

<sup>1</sup>W.R.M.L. and D.M.S. contributed equally to this work.

<sup>2</sup>To whom correspondence may be addressed. Email: [alvarezbuylla@ucsf.edu](mailto:alvarezbuylla@ucsf.edu).

This article contains supporting information online at <https://www.pnas.org/lookup/suppl/doi:10.1073/pnas.2313596120/-/DCSupplemental>.

Published January 29, 2024.

removal of the entire *Pcdhg* gene cluster did not affect the proliferation of cIN progenitors, or the migration and morphological complexity of cINs (33). Within the *Pcdhg* gene cluster, the sole deletion of *PcdhyC4*, but not that of other isoforms, is sufficient to cause neonatal lethality and increased cell death in the spinal cord (36). Whether *PcdhyC4* is the key isoform in the regulation of cIN survival remains unknown.

In the present study, we show that *PcdhyC4* was enriched in the cIN population and largely absent from excitatory neurons in the adult cortex. In contrast, the *PcdhyC5* isoform was mainly expressed in excitatory neurons. We observed that the expression of *PcdhyC4* in cINs and of *PcdhyC5* in excitatory neurons increased during the period of cIN PCD between postnatal day (P) 5 and P14. Using knockout mice in which various *Pcdhy* isoforms were deleted (36), combined with heterochronic transplantation (33), we then show that the 19 A- and B-type *Pcdhy* isoforms, as well as *PcdhyC3* and *PcdhyC5*, have minimal effect on cIN survival. In contrast, the deletion of *PcdhyC4* was sufficient to dramatically increase cell death among MGE-derived cINs during the normal period of PCD. Lastly, we showed that *Pcdhy*-deficient cINs were rescued from excess cell death by the viral overexpression of the *PcdhyC4* isoform. We conclude that *Pcdhy* diversity is not required for cIN survival; rather the expression of *PcdhyC4*, is necessary and sufficient for the survival of most cINs.

## Results

**Divergent Expression of *PcdhyC4* and *PcdhyC5* in cINs and Excitatory Cortical Neurons during PCD.** The *Pcdhg* gene locus encodes 22 distinct *Pcdhy* proteins, which are subclassified as A-, B-, or C-type isoforms. Previous work suggests that *Pcdhys* and specifically the C-type isoforms play a key role in the regulation of cIN PCD (33). This previous work suggested that either individual or multiple C-type *Pcdhys* are required to maintain appropriate numbers of cINs in the cortex. To determine whether differential expression patterns of individual C-type *Pcdhys* might be involved in cIN survival, we screened scRNA sequencing datasets to determine which C-type *Pcdhys* are expressed in cINs. Interestingly, two scRNA sequencing datasets generated from adult mice cortex (>P50) (37, 38) showed a distinct enrichment of *PcdhyC4* expression in GABAergic cells compared to excitatory cells. In contrast, glutamatergic excitatory neurons expressed higher levels of *PcdhyC5* (Fig. 1 *A* and *B*). Using these same datasets, we asked whether the expression of *PcdhyC4* and *PcdhyC5* differed in different subclasses of excitatory and inhibitory neurons (*SI Appendix, Fig. S1 A and B*). Among inhibitory neuron subtypes, interferon gamma-induced GTPase (*Igtp*), Neuron-derived neurotrophic factor (*Ndnf*), Parvalbumin (*Pvalb*), Somatostatin (*SST*), and Vasoactive intestinal peptide-expressing (*Vip*) cells showed a higher expression of *PcdhyC4* and lower levels of *PcdhyC5*. Among the excitatory neurons, higher levels of *PcdhyC5* expression were evident in deep and superficial glutamatergic neurons. Together, these scRNA-sequencing datasets indicate that the *PcdhyC4* and *PcdhyC5* genes are differentially expressed between cINs and excitatory neurons in the adult mouse cortex. In contrast, expression of *PcdhyC3*, which plays a unique role in promoting cortical dendrite arborization through its signaling partner *Axin1* (39), was expressed at low levels in both GABAergic and glutamatergic neurons, similar to that of the other *Pcdhy* genes (Fig. 1 *A* and *B*). Together, these observations suggest that *PcdhyC4* and *PcdhyC5* might play distinct functions in cINs and excitatory neurons, respectively.

In order to confirm the above observations in tissue sections, we performed in situ hybridizations using RNAscope in visual cortex

sections of *Nkx2.1;Ai6* mice in which MGE-derived cINs express the *ZsGreen* protein (40). Using probes against the *PcdhyC4* and *PcdhyC5* mRNA transcripts, we investigated the in vivo patterns of expression of these adhesion molecules during the period of PCD (P5, P7, and P14) (Fig. 1 *C* and *D*). At P5, 62.1% of *ZsGreen*<sup>+</sup> cINs were positive for *PcdhyC4*, increasing to 69.6% at P7 and to 89.4% by P14 (Fig. 1*E*). This suggests that by the onset of PCD, cINs already express *PcdhyC4*. However, measurements of the average mean intensity of *PcdhyC4* signal per cell indicate that the levels of *PcdhyC4* expression in MGE-derived cINs increased drastically during PCD (Fig. 1*F*). In contrast to the *ZsGreen*<sup>+</sup> MGE-derived cINs, only a small fraction of *ZsGreen*<sup>-</sup> cells expressed *PcdhyC4* (Fig. 1*F*). *ZsGreen*<sup>+</sup> MGE-derived cINs expressed no or low levels of *PcdhyC5* during the period of PCD (0.9% at P5, 6.8% at P7, and 8.5% at P14) (Fig. 1*G*). However, *ZsGreen*<sup>-</sup> cells frequently expressed high levels of *PcdhyC5* (Fig. 1*H*).

We further validated the expression of *PcdhyC5* in the cerebral cortex by immuno-staining. Staining for *PcdhyC5* was combined with *Cux1* and *Ctip2* immunostainings to identify upper and lower layer cortical excitatory neurons respectively (*SI Appendix, Fig. S1 C and D*). While no *PcdhyC5* signal was detectable at P5 and P7, *PcdhyC5* staining clearly surrounded 94.8% of *Cux1*<sup>+</sup> neurons and 81.5% of *Ctip2*<sup>+</sup> neurons at P14 (*SI Appendix, Fig. S1 H and I*). To determine whether *PcdhyC5* expression is lower in inhibitory neurons, we costained the visual cortex with *PcdhyC5* and *ZsGreen* antibodies in the *Nkx2.1;Ai6* P14 mice (*SI Appendix, Fig. S1 G*). Consistent with the scRNA-seq data, inhibitory neurons had visibly lower levels of *PcdhyC5* protein with only 11.2% of *ZsGreen* neurons expressing *PcdhyC5*. Additionally, we performed *PcdhyC5* stainings in combination with immunostaining for PV and SST (*SI Appendix, Fig. S1 E and F*). Among the MGE-derived cINs, 20.6% of PV cells and 30.0% of SST neurons were *PcdhyC5*<sup>+</sup> (*SI Appendix, Fig. S1 H and I*). Together, these data indicate divergent expression of *PcdhyC4* in cINs and *PcdhyC5* in excitatory neurons, with the levels of expression of *PcdhyC4* and *PcdhyC5* in these two neuronal populations increasing during the period of PCD. Immunostaining for *PcdhyC4* has not been reported and of the 5 antibodies (*Methods*) for *PcdhyC4* we tested, none worked for immunostaining.

***PcdhyC4* Deletion Results in the Elimination of Most cINs.** Our previous work has shown that the combined deletion of the three *Pcdhy* C-type genes (*PcdhyC3*, *PcdhyC4*, and *PcdhyC5*) results in increased cIN cell death during the period of naturally occurring PCD (33). A recent study has shown that constitutive genetic deletion of *PcdhyC4*, but not that of *PcdhyC3* or *PcdhyC5*, leads to neonatal lethality and increased interneuron cell death in the spinal cord (36). To ascertain the function of *PcdhyC4* in the regulation of cIN PCD, we transplanted cells from mice with a constitutive deletion of the *PcdhyC4* isoform (*Pcdhy*<sup>C4KO</sup> mice) (36). *Pcdhy*<sup>C4KO</sup> mice were crossed to the *Nkx2.1*<sup>Cre</sup>; *Ai14* MGE/preoptic area (POA) reporter mouse line to provide a genetically encoded fluorescent label for the cINs (Fig. 2*A*).

Embryos homozygous for deletion of the *PcdhyC4* isoform develop normally with no apparent weight, size, or brain abnormalities and are born in normal Mendelian ratios. However, these mice die perinatally (within 24 h of birth) before the period of PCD for cINs (P0–P15). In order to bypass lethality and to study the role of *PcdhyC4* deletion in cIN survival postnatally, we used a cotransplantation method; transplanting a mixture of WT cINs with mutant cINs (Fig. 2*B*). This allowed us to compare the survival of mutant and WT cells within the same WT environment. The F2 generation of *Nkx2.1*<sup>Cre</sup>; *Ai14*; *Pcdhy*<sup>C4KO/+</sup> mice were bred to generate E13.5 embryos, homozygous for the *Pcdhy*<sup>C4KO</sup> allele.



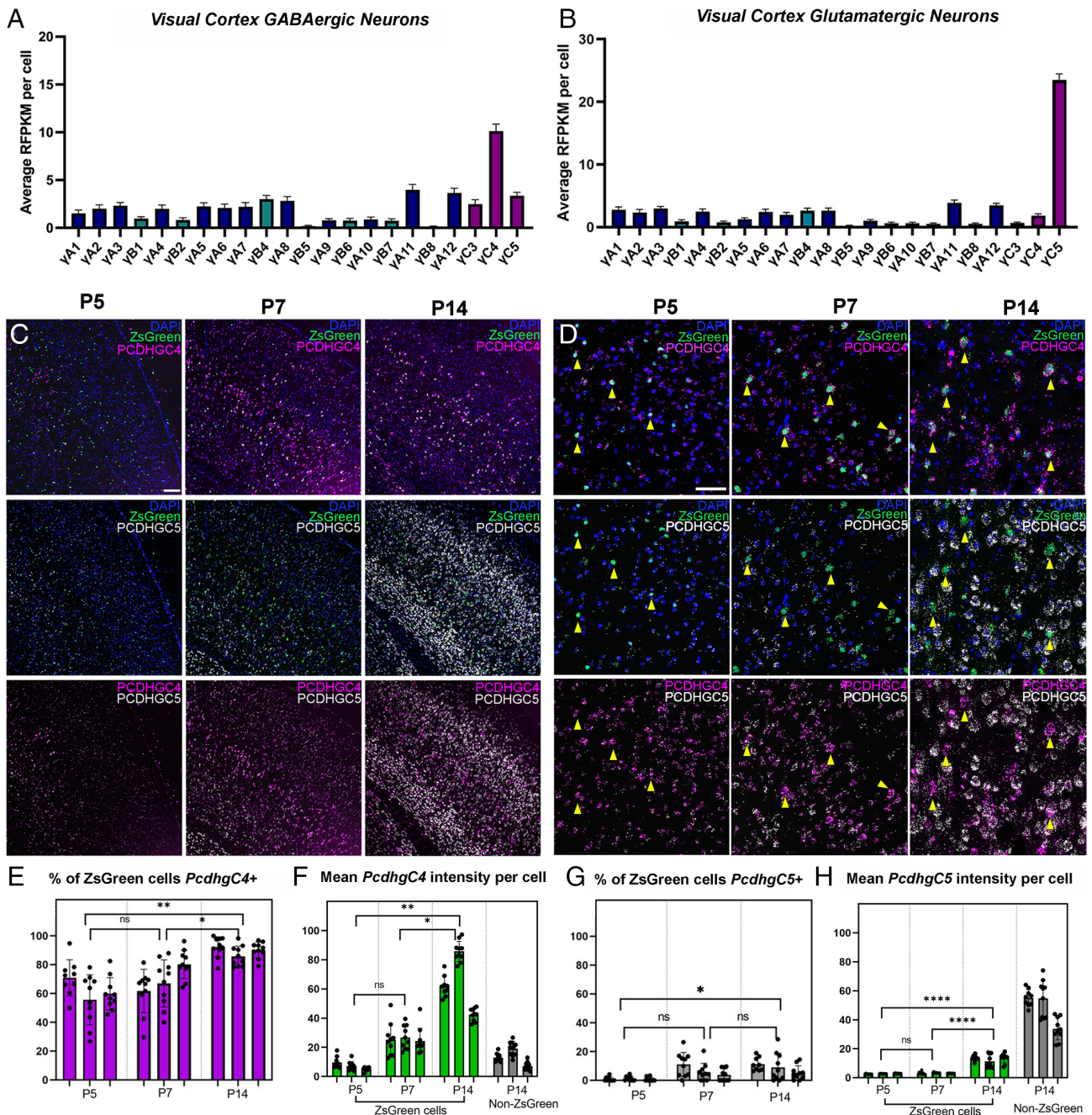


**Fig. 1.** Divergent expression of *Pcdhγ4* and *Pcdhγ5* in cINs and excitatory cortical neurons during PCD. (A and B) ScRNA-seq analysis from publicly available datasets (37, 38) shows high expression of *Pcdhγ4* in GABAergic cINs (A) and low expression in excitatory GLUTamatergic neurons (B). In contrast, *Pcdhγ5* is expressed high in excitatory neurons (B) and low in cINs (A). Error bars represent the SEM. (C and D) RNAscope of visual cortex in *Nkx2.1; Ai6* mice during PCD. Low (C) and high magnification (D) images show low expression of *Pcdhγ4* and *Pcdhγ5* at P5. Between P7 and P14, expression of both *Pcdhγ4* and *Pcdhγ5* has noticeably increased. By P7 and P14, *Pcdhγ4* is highly and preferentially expressed in ZsGreen<sup>+</sup> MGE-derived cINs (yellow arrows), while *Pcdhγ5* is preferentially present in ZsGreen<sup>-</sup> cells. Scale bar low-magnification (C) = 100 μm. Scale bar high-magnification (D) = 50 μm. (E and F) Quantification of *Pcdhγ4* *isoform* transcripts in the visual cortex of P5–P14 mice (E). Measurements of the average mean signal intensity of *Pcdhγ4* in ZsGreen<sup>+</sup> MGE-derived cINs showing *Pcdhγ4* signal increases significantly between P5 and P14, while expression of *Pcdhγ4* in ZsGreen<sup>-</sup> MGE-derived cells remains comparably low (F). *n* = 3 animals per genotype, 9 to 10 fields per animal, quantified at least 25 cells per field. Nested 1-way ANOVA with Tukey's multiple comparisons test; \**P* < 0.05, \*\**P* < 0.01, \*\*\**P* < 0.005, and \*\*\*\**P* < 0.0001; ns = not significant. (G and H) Quantification of *Pcdhγ5* *isoform* transcripts in the visual cortex of P5–P14 mice. Proportions of MGE-derived cINs that express *Pcdhγ5* remained low during the period of PCD; 0.9% at P5, 6.8% at P7, and 8.5% at P14 (G). The average mean signal intensity of *Pcdhγ5* transcript in MGE-derived cINs was low throughout PCD, while non-MGE (ZsGreen<sup>-</sup>) derived cINs showed high *Pcdhγ5* signal at P14 (H). *n* = 3 animals per genotype, 9 to 10 fields per animal, quantified at least 25 cells per field. Nested 1-way ANOVA with Tukey's multiple comparisons test; \**P* < 0.05, \*\**P* < 0.01, \*\*\**P* < 0.005, and \*\*\*\**P* < 0.0001; ns = not significant.

In these embryos, MGE/POA-derived cells lacking *Pcdhγ4* are fluorescently labeled with the tdTomato protein upon Cre-driven recombination of the *Ai14* allele.

The MGEs of embryos carrying the homozygous deletion of the *Pcdhγ4* allele were microdissected. As a control, green fluorescent

protein (GFP)-expressing cINs were obtained from microdissected MGEs of *Nkx2.1<sup>Cre</sup>; Ai6* mice, in which MGE-POA-derived cells are fluorescently labeled with ZsGreen (40) (Fig. 2 A and B) or *Gad67-GFP* embryos (SI Appendix, Fig. S2 A and B). The MGEs were dissociated, and cells were mixed in similar proportions (GFP



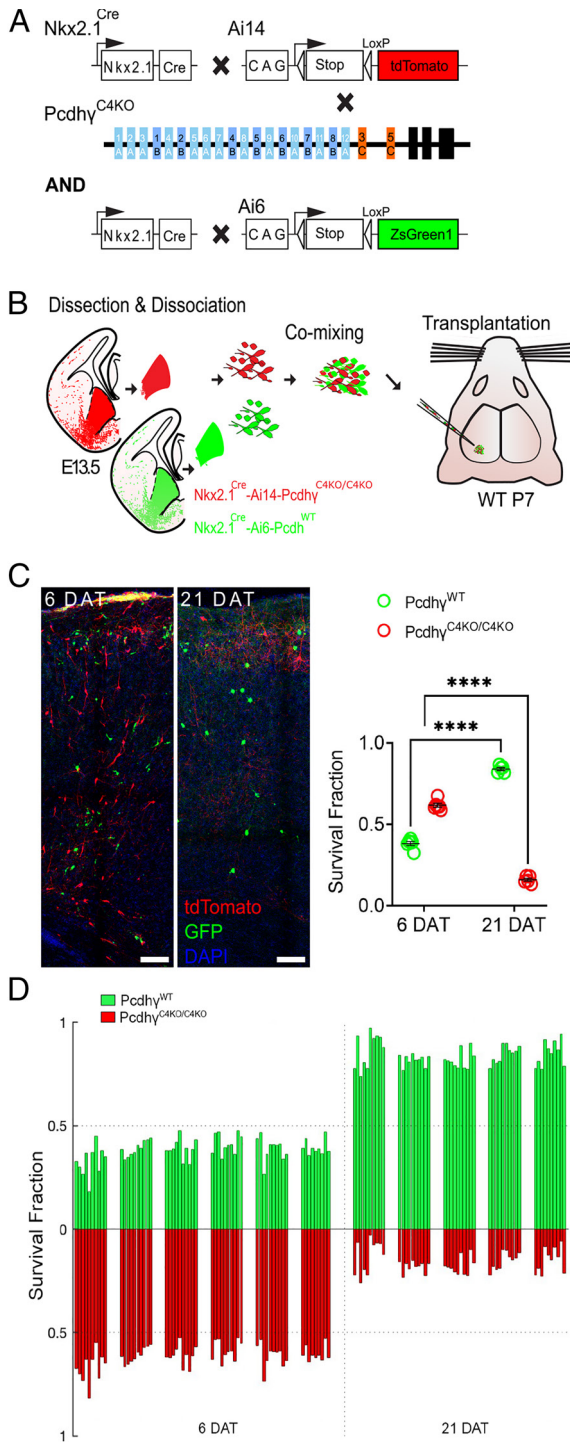


**Fig. 2.** Genetic deletion of *PcdhyC4* increased cell death in MGE-derived cINs. (A) Diagram of genetic crosses between MGE/POA-specific reporter and  $Pcdhy^{C4KO}$  mice.  $Pcdhy^{C4KO}$  homozygous MGE cells were obtained from the  $Nkx2.1^{Cre}; Ai14; Pcdhy^{C4KO/C4KO}$  embryos, whereas control cells were obtained from  $Nkx2.1^{Cre}; Ai6$  embryos. (B) Schematics of transplantation protocol. The MGEs from E13.5  $Pcdhy^{C4KO}$  homozygous mutant or control embryos were dissected, dissociated, and mixed in similar proportions. The mixture of GFP<sup>+</sup> ( $Pcdhy^{WT}$ ) and tdTomato<sup>+</sup> ( $Pcdhy^{C4KO/C4KO}$ ) cells was grafted into the cortex of WT neonate mice. (C) *Left*—Confocal images from the cortex of mice at 6 and 21 DAT. The transplanted cells are labeled with GFP ( $Pcdhy^{WT}$ ) or tdTomato ( $Pcdhy^{C4KO/C4KO}$ ). *Right*—Quantifications (shown as survival fraction) of surviving MGE-derived cINs at 6 and 21 DAT. Both the transplanted GFP and tdTomato-labeled cells undergo PCD between 6 and 21 DAT, but the  $Pcdhy^{C4KO/C4KO}$  cells are eliminated at significantly higher rates. (D) Survival fraction quantifications from (C) shown by individual brain sections (each bar) and separated by animals at 6 and 21 DAT. Scale bar = 50  $\mu m$ , nested ANOVA, \*\*\*\* $p = 3.147 \times 10^{-10}$ ,  $n = 5$  mice per time point and 10 brain sections quantified per mouse, DAT 6 cells counted = 9,125, DAT 21 cells counted = 3,125.

and tdTomato). The mixture of GFP cells with tdTomato cells was transplanted into the cortex of host neonatal mice (P3–P7). The homozygous  $Pcdhy^{C4KO/C4KO}$  cells were identified via tdTomato expression while cells carrying the  $Pcdhy^{WT}$  allele were identified via expression of GFP (Fig. 2C). Survival of the transplanted cells was analyzed at 6 and 21 d posttransplant (DAT), which corresponds to postnatal days (P) 0 and 15 for the transplanted cells, cellular ages that span the period of endogenous cIN PCD. At 6 DAT, the proportion of the fluorescently labeled transplanted cells expressing GFP ( $Pcdhy^{WT}$ ) was 38.2%, and the tdTomato-positive  $Pcdhy^{C4KO/C4KO}$  cells made up the balance, 61.8%, of all transplanted cells that survived. Importantly, there was no apparent change in the proportion of GFP to tdTomato cells between 4 and 6 DAT (SI Appendix, Fig. S3A), before the period of naturally occurring cell death for the transplanted cells. By 21 DAT, however, the proportion of GFP to tdTomato cells had shifted dramatically, indicating that one cell population was eliminated at higher rates. Indeed, the tdTomato-positive  $Pcdhy^{C4KO/C4KO}$  cell population dropped from 61.8% (at 6 DAT) to 15.9% at 21 DAT. Conversely, the proportion of GFP-positive  $Pcdhy^{WT}$  cINs had increased from 38.2% (at 6 DAT) to 84.1% at 21 DAT. Note that the increase in the proportion of GFP-positive cells does not reflect an increase in survival, but rather that the tdTomato-labeled cells were eliminated in much greater numbers during PCD. Importantly, similar but less robust reductions were found in experiments where we cotransplanted  $Pcdhy^{C4KO/C4KO}$  with  $Pcdhy^{WT}$  cells derived from *Gad67*-GFP embryos (SI Appendix, Fig. S2). These differences in survival proportions could be due to contributions from non-*Nkx2.1*-derived cINs (*Gad67*-GFP<sup>+</sup> cINs derived from the CGE that migrate through the MGE or those derived from the dorsal MGE that do not express *Nkx2.1*). These results suggest that cells that lack the *PcdhyC4* protein are more likely to be eliminated during the normal period of cell death than those cells that express the WT *PcdhyC4*.

**Deletion of All *Pcdhy*, Except *PcdhyC4*, Is Sufficient for the Survival of the Majority of cINs.** We wondered whether *PcdhyC3* and *PcdhyC5* may also contribute to cIN survival. In our previous study, deletion of the C-type isoforms (*PcdhyC3*, *PcdhyC4*, and *PcdhyC5*) resulted in the elimination of most cINs, to levels similar to those observed after the loss of function of the entire *Pcdhy* cluster (33). These suggested that the 19 alternate A- and B-type *Pcdhy* isoforms do not significantly contribute to the survival of cINs. Here, we used the  $Pcdhy^{IR1}$  mouse line (36), which lacks all 19 A- and B-type *Pcdhy* isoforms, as well as *PcdhyC3* and *PcdhyC5*, but retains *PcdhyC4* (Fig. 3A).

Mice homozygous for the  $Pcdhy^{IR1}$  allele ( $Pcdhy^{IR1/IR1}$ ) are born in normal mendelian ratios, develop normally, and are fertile, as previously reported (36).  $Pcdhy^{IR1/IR1}$  mice were crossed to the above  $Nkx2.1^{Cre}; Ai14; Pcdhy^{C4KO/C4KO}$  mouse line to label MGE/POA-derived cINs with the tdTomato protein (Fig. 3A). As above, we used cotransplantation to compare the survival of cINs solely expressing *PcdhyC4* to that of cINs expressing all 22 *Pcdhy* isoforms. cIN precursor cells homozygous for the  $Pcdhy^{IR1/IR1}$  allele were obtained from E13.5  $Nkx2.1^{Cre}; Ai14; Pcdhy^{IR1/IR1}$  embryos. As a control, we used cIN precursor cells expressing WT *Pcdhy* obtained from  $Nkx2.1^{Cre}; Ai6$  embryos (Fig. 3B). Survival of the transplanted cells was analyzed at 6 and 21 DAT and is represented as the proportion of GFP to tdTomato cells at these time points. At 6 DAT, roughly 44.7% of all transplanted cells were GFP-positive (WT *Pcdhy*) while the remaining cells (55.2%) were tdTomato-positive ( $Pcdhy^{IR1/IR1}$ ). As hypothesized, the survival of the  $Pcdhy^{IR1/IR1}$  tdTomato positive cells was remarkably similar to that of the GFP-labeled control cells (Fig. 3C and D). However,

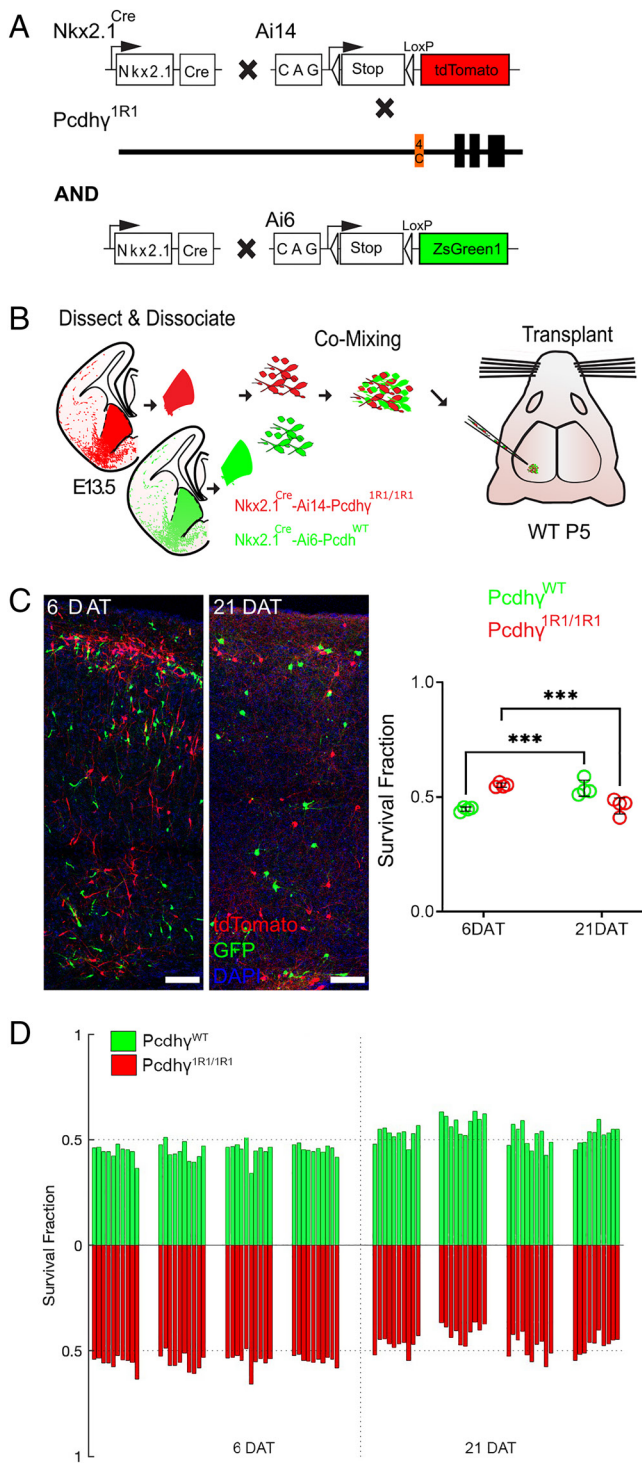


**Fig. 3.** Most MGE-derived cINs survive the deletion of most *Pcdhy*, except for *PcdhyC4*. (A) Diagram of genetic crosses between MGE/POA-specific reporter  $Nkx2.1^{Cre}; Ai14$  and  $Pcdhy^{1R1/1R1}$  mice. Control cells were derived from  $Nkx2.1^{Cre}; Ai6$  mice while  $Pcdhy^{1R1/1R1}$  mutant cells were derived from  $Nkx2.1^{Cre}; Ai14; Pcdhy^{1R1/1R1}$  mice. (B) Diagram of the transplantation protocol. The MGEs from E13.5  $Pcdhy^{1R1/1R1}$  homozygous or control embryos were dissected, dissociated, and mixed in similar proportions. The mixture of GFP<sup>+</sup> ( $Pcdhy^{WT}$ ) and tdTomato<sup>+</sup> ( $Pcdhy^{1R1/1R1}$ ) cells was grafted into the cortex of WT neonate mice. (C) Left—Confocal images from the cortex at 6 and 21 DAT. The transplanted cells are labeled with GFP ( $Pcdhy^{WT}$ ) or tdTomato ( $Pcdhy^{1R1/1R1}$ ). Right—Quantifications of the transplanted cells that survived at 6 and 21 DAT. Note that both the GFP and tdTomato labeled cells underwent PCD between 6 and 21 DAT, but both cell types survived to similar levels. (D) Survival fraction quantifications from (C) shown by individual brain sections (each bar) and separated by animals at 6 and 21 DAT. Scale bar = 50  $\mu m$ , nested ANOVA, \*\*\* $P = 0.0026$ ,  $n = 4$  mice per time point and 10 brain sections per mouse. DAT 6 cell counted = 11,063, DAT 21 cells counted = 7,751.

there was a small but significant drop in the  $Pcdhy^{1R1/1R1}$  population (9.1%), as compared to a 45.9% decrease in the  $Pcdhy^{C4KO/C4KO}$  transplants (Fig. 2 C and D). Similar results were observed when control cINs cells were obtained from the  $Gad67$ -GFP mouse line (SI Appendix, Fig. S4). Importantly, the proportion of GFP to tdTomato positive cells remained unchanged between 4 to 6 DAT (SI Appendix, Fig. S3B). Together, these data suggest that expression of *PcdhyC3* or *PcdhyC5* is not required for the survival of most cINs. Furthermore, these observations suggest that A- and B-type *Pcdhy* isoforms are also not required for cIN survival. Given the small drop in cIN survival in  $Pcdhy^{1R1/1R1}$  cIN, we cannot rule out the possibility that these A- and B-type *Pcdhy* isoforms, or *PcdhyC3* or *PcdhyC5* may make a small contribution to cIN survival. Alternatively, or in addition, decreased levels of *PcdhyC4* expression in the  $Pcdhy^{1R1/1R1}$  mice compared to WT mice (36) could explain the observed small but statistically significant drop in the survival.

**Exogenous Expression of *PcdhyC4* in *Pcdhy* Knockout cINs Rescues cINs from Cell Death.** The results above suggest that most cINs lacking expression of *PcdhyC4* are eliminated during the normal period of PCD; in contrast, cINs expressing *PcdhyC4* as their only *Pcdhy* isoform survive at nearly normal levels. We next asked whether cINs lacking expression of all 22 *Pcdhy* isoforms could be rescued from cell death by reintroducing the *PcdhyC4* isoform. Since cINs lacking the function of all *Pcdhy* isoforms are nearly eliminated when cotransplanted with WT cINs expressing *Pcdhy* (see figure 10E in ref. 33), we reasoned that a rescue effect would be most evident in these mutant cells.

To address whether exogenous expression of *PcdhyC4* is able to rescue cINs lacking the function of all *Pcdhy* isoforms, we created lentiviral constructs to express GFP alone or fused to the *PCDH $\gamma$ C4* molecule (*PCDH $\gamma$ C4*-GFP). We first validated these constructs using in vitro cultures of MGE-derived cINs (SI Appendix, Fig. S5). MGE cells from E13.5  $Nkx2.1^{Cre}; Ai14$  embryos that expressed WT *Pcdhy* were cocultured with cortical feeder cells of equivalent age, and infected with lentivirus to express the control GFP or *PCDH $\gamma$ C4* fused to the GFP. Expression of GFP alone or *PCDH $\gamma$ C4* fused to GFP was analyzed at 3, 5, 7, 9, or 11 d in vitro (DIV) (SI Appendix, Fig. S5A). MGE-derived cells infected with lentivirus and expressing lentiviral-driven GFP or *PCDH $\gamma$ C4*-GFP were positive for both tdTomato and GFP signals. GFP signal filled the whole cell area in the control experiment where the cells were infected with control lentivirus to express the GFP protein alone (SI Appendix, Fig. S5 B, Left). In contrast, the lentiviral driven *PCDH $\gamma$ C4*-GFP protein appeared to be preferentially localized to the cell surface, but it was also found in the cell soma, perisomatic regions, as well as in the axons and dendrites of cells infected with lentivirus expressing *PCDH $\gamma$ C4*-GFP (SI Appendix, Fig. S5 B, Right). Additionally, western blot analysis of neuronal cultures infected with lentivirus expressing either GFP or *PCDH $\gamma$ C4*-GFP revealed the presence of GFP-positive bands at the expected sizes of approximately 26 kD and 130 kD, respectively (SI Appendix, Fig. S5C).

Dissociated MGE cells from E13.5 of  $Nkx2.1^{Cre}; Ai14; Pcdhy^{fcon3/fcon3}$  embryos were infected in suspension with lentivirus expressing the *PcdhyC4* isoform fused to GFP (Fig. 4 A and B). The infected cells were transplanted into WT host neonate mice and survival was analyzed at 6 and 21 DAT. The transplanted cINs expressing lentivirus-driven *PcdhyC4* were identified via the coexpression of tdTomato and GFP (Fig. 4 C). *Pcdhy* mutant cells that expressed only tdTomato were identified as not infected. We compared the survival of *PcdhyC4*-transduced (tdTomato<sup>+</sup>GFP<sup>+</sup>) to nontransduced (tdTomato<sup>+</sup>GFP<sup>-</sup>) at 6 and 21 DAT. While both



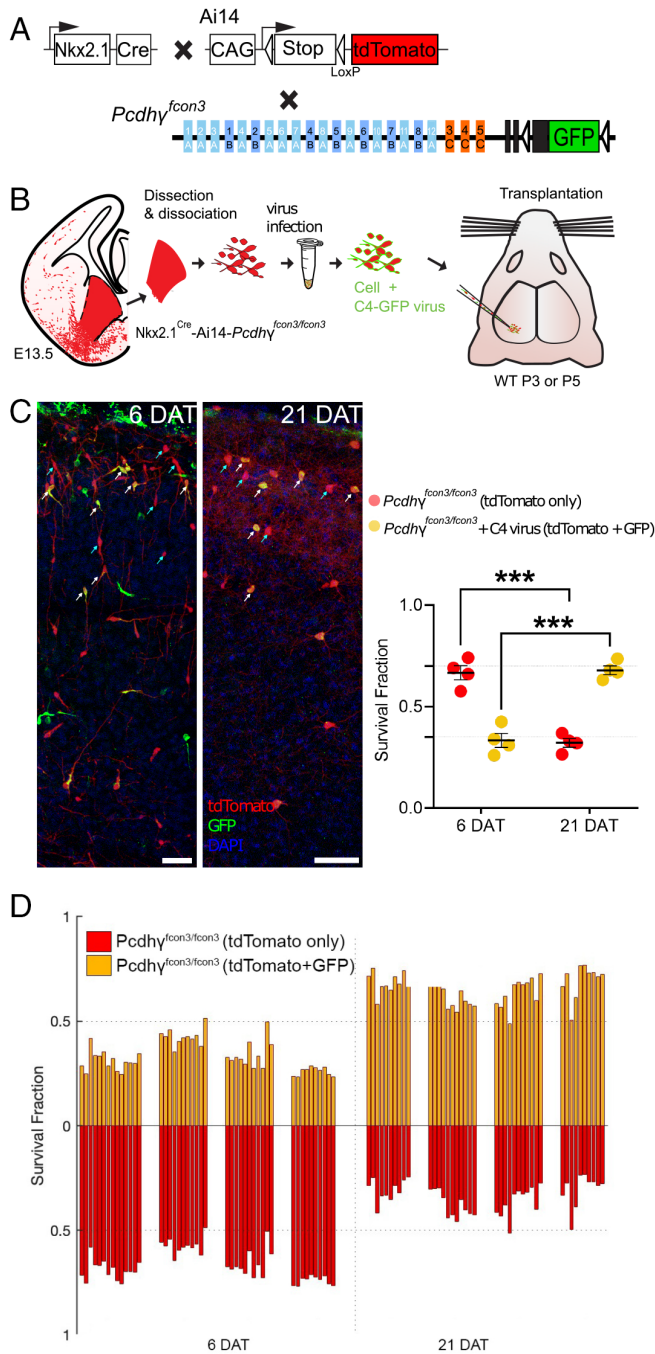


**Fig. 4.** Lentiviral expression of PcdhyC4 rescues cINs with Pcdhy loss of function. (A) Diagram of mouse genetic crosses. Pcdhy<sup>fcon3</sup> mice were crossed to the Nkx2.1<sup>Cre</sup>;Ai14 mouse line to generate embryos with loss of function of all Pcdhy isoforms. (B) Schematic of the lentiviral infection and transplantation of MGE cIN precursors. The MGEs of Nkx2.1<sup>Cre</sup>;Ai14;Pcdhy<sup>fcon3/fcon3</sup> embryos were dissected, dissociated, and infected in suspension with lentivirus carrying PcdhyC4-GFP. The mixture of transduced and nontransduced cells was grafted into the cortex of WT neonate recipient mice. (C) Confocal images of the transplanted cINs in the cortex at 6 and 21 DAT. Notice the expression of GFP can be found near the cell surface including the cell processes, reflecting the putative location of the transduced PcdhyC4-GFP protein. Quantifications of the tdTomato<sup>+</sup>GFP<sup>+</sup> (red cells, teal arrows) or tdTomato<sup>+</sup>GFP<sup>-</sup> (yellow cells, white arrows) cells are shown as the fraction of cells from the total tdTomato<sup>+</sup> cells at 6 and 21 DAT. The fraction of the PcdhyC4-transduced yellow cells increases from 6 to 21 DAT, while the fraction of nontransduced (tdTomato<sup>+</sup>GFP<sup>-</sup>) decreases at equivalent time points. (D) Survival fraction quantifications from (C) shown by individual brain sections (each bar) and separated by animals at 6 and 21 DAT. Scale bar = 50 μm, nested ANOVA, \*\*\*\*P = 0.0002, n = 4 mice per time point and 10 brain sections per mouse from one transplant cohort. DAT 6 cell counted = 15,071, DAT 21 cells counted = 1,660.

the PcdhyC4-transduced and nontransduced cINs underwent a wave of cell death between the above time points, the fraction of tdTomato<sup>+</sup>GFP<sup>+</sup> cells increased between 6 and 21 DAT (33% to 68%). In contrast, the fraction of tdTomato<sup>+</sup>GFP<sup>-</sup> cells decreased from 66% to 32% during the same period of time (Fig. 4C). To control for possible nonspecific effects of viral infection on cIN survival, we infected Nkx2.1<sup>Cre</sup>;Ai14 MGE cells that carry the WT Pcdhy allele with lentivirus expressing GFP, and analyzed their survival at 6 and 21 DAT (SI Appendix, Fig. S6 A and B). As above, we compared the survival of PcdhyC4-transduced (tdTomato<sup>+</sup>GFP<sup>+</sup>) to nontransduced (tdTomato<sup>+</sup>GFP<sup>-</sup>) cells. At 6 DAT, the fraction of infected cells was approximately 50% and remained nearly constant between 6 and 21 DAT, indicating that infection with lentivirus and expression of GFP had no impact on cIN survival (SI Appendix, Fig. S6 C and D). These results indicate that the introduction of PcdhyC4 to cINs lacking endogenous Pcdhy genes is sufficient to rescue the mutant cells from undergoing excessive apoptosis.

## Discussion

This study reveals that MGE-derived cINs preferentially expressed PcdhyC4, and excitatory neurons preferentially expressed PcdhyC5. This segregated pattern of expression developed during the period of PCD. We show that loss of PcdhyC4 isoform, but not of the other 21 Pcdhy isoforms, resulted in a dramatic increase in MGE-derived cIN elimination. Furthermore, lentiviral mediated expression of PcdhyC4 was sufficient to rescue the survival of MGE-derived cells that lack the function of the entire Pcdhy cluster. PcdhyC4 appears to be the relevant Pcdhy involved in the regulation of MGE-derived cIN survival. During the period of PCD for cIN, local inhibitory networks facilitate synchronous activity which promotes interneuron survival (25). PcdhyC4 could be key in the formation of these early cortical networks that determine which cINs survive.

Previous studies show that Pcdhy C-type isoforms (PcdhyC3, PcdhyC4, and PcdhyC5) are required to regulate neuronal numbers during the critical window of PCD (33, 41). Members of the Pcdhy cluster have been shown to be key for neuronal survival, not only among cINs, but also in spinal cord and retina (35, 36, 42, 43). Indeed, a recent study reported that deletion of PcdhyC4, but not of other Pcdhy isoforms, leads to increased cell death in the spinal cord and to neonatal lethality (36). In contrast to spinal cord, where most PCD occurs prenatally (36, 42, 43), PCD of cINs in mice occurs postnatally. Since mice lacking PcdhyC4 (Pcdhy<sup>C4KO</sup>) die soon after birth, we could not study the extent of cIN cell death directly in these mutant animals. Instead, we used heterochronic transplantation to bypass this lethality and compare the survival of cINs lacking PcdhyC4 with cells that carry all Pcdhy isoforms. Pcdhy<sup>C4KO</sup> mice lack expression of PcdhyC4 but express the 19 A- and B-type Pcdhy isoforms as well as PcdhyC3 and PcdhyC5. In transplanted cINs that lack expression of PcdhyC4, the timing and extent of cIN elimination were similar to those observed when the entire Pcdhy gene cluster, or the Pcdhy C-type isoforms, are deleted (33). The above finding suggests that C-type isoforms PcdhyC3 and PcdhyC5 do not play a major role in the regulation of cIN survival; this is consistent with the relatively low expression of these isoforms in cINs. While PcdhyC5 was preferentially expressed by excitatory neurons, the expression of this Pcdhy isoform only increased well after the peak of PCD in this cell population (P4) (18). This observation, along with previous reports in which the loss of function of the entire Pcdhy cluster is directed to the excitatory neurons, suggests that



Pcdh $\gamma$ C5 does not play a role in the regulation of PCD in excitatory neurons (31, 44).

In agreement with the above findings, when we studied the survival of cINs that solely expressed Pcdh $\gamma$ C4 using cells from Pcdh $\gamma$ <sup>1R1</sup> embryos, we found that the majority of cINs survived. However, these transplanted Pcdh $\gamma$ <sup>1R1</sup> cINs did show a small but significant reduction in survival, compared to control cells. While we cannot completely exclude a role for other Pcdh $\gamma$  isoforms, including Pcdh $\gamma$ C3 or Pcdh $\gamma$ C5 in the Pcdh $\gamma$ <sup>1R1</sup> cells, the observed reduction in survival is likely due to reduced levels of Pcdh $\gamma$ C4 expression in Pcdh $\gamma$ <sup>1R1</sup> mice (36). To complement the above findings from the Pcdh $\gamma$ <sup>1R1</sup> experiments, we expressed the Pcdh $\gamma$ C4 isoform via lentivirus in cINs that lack expression of all 22 Pcdh $\gamma$  isoforms. Expression of Pcdh $\gamma$ C4 resulted in a dramatic increase in the survival of MGE-derived cINs lacking the function of the entire Pcdh $\gamma$  gene cluster. Our findings suggest that Pcdh $\gamma$  diversity is not required for the survival of cINs and show a unique role for Pcdh $\gamma$ C4 in regulating the survival of MGE-derived cINs. While the Pcdh $\gamma$  cluster is also important for the survival of CGE-derived cINs (33, 44), it remains unknown whether Pcdh $\gamma$ C4 is also the key isoform for regulation of PCD among these cINs.

Together, our results align with findings in the spinal cord and retina (36, 41), suggesting a potential general Pcdh $\gamma$ C4-driven mechanism that regulates the survival of local-circuit neurons across the CNS. While our data suggest that Pcdh $\gamma$  diversity is dispensable for cIN survival, the Pcdh $\alpha$  and Pcdh $\beta$  gene clusters remained intact and these Pcdhs could have contributed to diversity. A recent study found that mutant mice lacking all Pcdh $\alpha$ , Pcdh $\beta$ , and A- and B-type Pcdh $\gamma$  genes (thus retaining only Pcdh $\gamma$ C3, Pcdh $\gamma$ C4, and Pcdh $\gamma$ C5), also exhibited neonatal lethality and increased neuronal apoptosis (45). This observation could be explained by non-mutually exclusive scenarios: 1) the formation of Pcdh $\gamma$ C4 heterodimers, *in cis*, with members of Pcdh $\alpha$  and/or Pcdh $\beta$  clusters, providing cellular specificity important for cIN survival; and/or 2) that Pcdh $\gamma$ C4 (uniquely among Pcdh $\gamma$  isoforms) requires other clustered Pcdhs to be transported to the cell surface (46). While the mutant mice used by Kobayashi et al. (45) retain Pcdh $\gamma$ C3 and Pcdh $\gamma$ C5, these isoforms are expressed at low levels in cINs. In addition, it has been shown that *cis*-interactions among C-type Pcdhs are weak and this may prevent Pcdh $\gamma$ C3 and Pcdh $\gamma$ C5 from functioning as carriers for Pcdh $\gamma$ C4 (47). The removal of the Pcdh $\alpha$  or Pcdh $\beta$  clusters alone does not significantly affect cIN survival (33). Still, it remains unknown whether, in the absence of other members of the Pcdh $\gamma$  cluster, Pcdh $\gamma$ C4 requires members of Pcdh $\alpha$  or Pcdh $\beta$  clusters to regulate cIN survival. Whereas our data indicate a key role for Pcdh $\gamma$ C4 in the regulation of PCD among cINs, the mechanisms by which the Pcdh $\gamma$ C4 isoform regulates cIN survival remain unknown. Interestingly, Pcdh $\gamma$ C3 promotes cortical pyramidal neuron dendritic arborization through its intracellular interactions with Axin1 (39). It will be interesting to investigate whether Pcdh $\gamma$ C4 has similar and unique cytoplasmic interactors influencing signaling pathways involved in neuronal survival.

This work, along with previous studies, suggests that the final number of cINs in the cerebral cortex is in part determined through a cell- or population-intrinsic mechanism involving cell-cell interactions among cINs of the same age (11). Given the key role Pcdh $\gamma$ C4 plays in the survival of cINs and the fact that Pcdh $\gamma$ C4 is a cell-adhesion molecule that is involved in homophilic cell-cell recognition (46), initial cell-cell interactions within the cIN population could be mediated through Pcdh $\gamma$ C4. Other studies have shown that PCD is also regulated, at least in part, through activity-dependent mechanisms (18, 25, 48). It remains undetermined what role, if any, Pcdh $\gamma$ C4 plays in the regulation

of activity during the peak of PCD. In this regard, it would be interesting to determine whether network activity is perturbed in cINs lacking Pcdh $\gamma$ C4. Interestingly, loss of vesicular GABA release from cINs and the resulting reduction in inhibition leads to their increased participation in network activity and increased cIN survival (25). The epistatic relationship between vesicular GABA release and the function of Pcdh $\gamma$ C4 in cINs in the regulation of PCD remains to be determined.

Appropriate numbers of cINs are considered essential in the modulation of cortical function. This is ultimately adjusted by a period of PCD once the young cINs have migrated into the cortical plate and have begun to make synaptic connections. In postmitotic neurons of the peripheral nervous system, neurons are eliminated extrinsically, through competition for limiting signaling neurotrophic factors (49, 50). PCD in cINs correlates with the age of the cells, suggesting that it is in part regulated by their maturation program. Here, we show that as part of this maturation, cINs increase expression of Pcdh $\gamma$ C4 and show that this Pcdh is an essential molecular component in the regulation of MGE-derived cIN PCD. Interestingly, mutations in the Pcdh $\gamma$ C4 gene are associated with progressive microcephaly and seizures (51), suggesting that the Pcdh $\gamma$ C4 isoform also plays a key role in IN survival in the human cortex. An understanding of the cell-cell interactions that use Pcdh $\gamma$ C4 to regulate cIN cell death should provide fundamental insights into how the cerebral cortex forms and evolves.

## Methods

**Animals.** All protocols and procedures followed the University of California, San Francisco (UCSF) guidelines and were approved by the UCSF Institutional Animal Care Committee. The following breeders were purchased from the Jackson Laboratory: Ai6, Ai14, Gad1-GFP, *BAC-Nkx2.1-Cre* (Nkx2.1<sup>Cre</sup>), and WT C57BL/6 J. Pcdh $\gamma$ -fcon3 (FCON3) mice were obtained from Joshua Sanes at Harvard University. Pcdh $\gamma$ <sup>1R1/1R1</sup> (1R1), Pcdh $\gamma$ <sup>C4KO/C4KO</sup> (C4KO), and Pcdh $\gamma$ <sup>3R2/3R2</sup> (3R2) mice were transferred from the Weiner laboratory at the University of Iowa, rederived, and bred at UCSF.

Pcdh $\gamma$  loss of function mice were obtained by crossing Pcdh $\gamma$ <sup>fcon3/fcon3</sup> mice with Nkx2.1<sup>Cre</sup>-Ai14-Pcdh $\gamma$ <sup>fcon3/+</sup>. Pcdh $\gamma$ <sup>1R1/1R1</sup> (1R1) and Pcdh $\gamma$ <sup>C4KO/+</sup> (C4KO) mice were crossed to Nkx2.1<sup>Cre</sup>-Ai14 breeders to label the Nkx2.1 progenitor cells.

For cell transplantation experiments, GFP-expressing MGE-derived cells were produced by crossing WT C57BL/6 J to heterozygous mice expressing GFP driven by Gad1 or by crossing Nkx2.1<sup>Cre</sup>;Ai6 breeders to WT C57BL/6 J mice. For all tdTomato-expressing cells derived from MGE embryonic microdissections, we crossed the various mutant alleles to the Nkx2.1<sup>Cre</sup>-Ai14 line. Pcdh $\gamma$ <sup>fcon3/fcon3</sup> mutant embryonic tissue was obtained from embryos produced by crossing Nkx2.1<sup>Cre</sup>-Ai14-Pcdh $\gamma$ <sup>fcon3/+</sup> mice with Pcdh $\gamma$ <sup>fcon3/fcon3</sup> mice. Pcdh $\gamma$ <sup>1R1/1R1</sup> mutant tissue was obtained from embryos produced by crossing Nkx2.1<sup>Cre</sup>-Ai14-Pcdh $\gamma$ <sup>1R1/1R1</sup> breeders. Pcdh $\gamma$ <sup>C4KO/C4KO</sup> mutant tissue was obtained from embryos produced by crossing Nkx2.1<sup>Cre</sup>-Ai14-Pcdh $\gamma$ <sup>C4KO/+</sup> breeders. Gad1-GFP, Nkx2.1<sup>Cre</sup>; Ai6, and Nkx2.1<sup>Cre</sup>-Ai14 offspring were genotyped under an epifluorescence microscope (Leica), and PCR genotyping was used to screen for Pcdh $\gamma$ <sup>fcon3/fcon3</sup>, Pcdh $\gamma$ <sup>1R1/1R1</sup>, and Pcdh $\gamma$ <sup>C4KO/C4KO</sup> alleles in tdTomato positive embryos or reporter negative embryos. All cell transplantation experiments were performed using wild-type C57BL/6 recipient mice P2 to P8. All mice were housed under identical conditions.

**Plasmids.** The following plasmids were used in this work: pLenti-CAG-EGFP and pLenti-CAG-Pcdh $\gamma$ C4-EGFP.

**Timed pregnant mice.** In experiments requiring timed pregnant mice, the day when the sperm plug was observed was considered E0.5. Males were paired with females the night before and checked for plugs early the following day. MGE cells for transplantation were dissected from the fetal forebrain between E12.5 and E15.5 embryos as previously described (11).

**Transplantation.** For cotransplantation experiments, the concentration of cells of each genotype was determined using a hemocytometer; the GFP or tdTomato-labeled cells were then mixed in similar proportions. To prepare the cells for transplantation, the cell suspension was concentrated by spinning in a

table centrifuge for 5 min at 800g (rcf). The supernatant was removed, and the resulting pellet was resuspended and mixed in a final volume of 1 to 6  $\mu$ L of Leibovitz L-15 medium (L15). This concentrated cell suspension was loaded into beveled glass micropipettes (~60 to 100  $\mu$ m diameter, Wiretrol 5  $\mu$ L, Drummond Scientific Company) prefilled with mineral oil and mounted on a microinjector as previously described (52). The viability and concentration of the cells in the glass micropipette were determined by using 100 nL of cells diluted 200X in 10  $\mu$ L of L15 medium and 10  $\mu$ L trypan blue. The number of cells was then determined using a hemocytometer. Cells were injected into neonate mice P3 to P7. Prior to the injection of cells, the recipient mice (C57Bl/6) were anesthetized by hypothermia (~3 to 5 min) and positioned in a clay head mold that stabilizes the skull (53). Micropipettes were positioned at an angle of 0 or 30 degrees from vertical in a stereotactic injection apparatus, and injected between 4 to 6 mm A/P and 0.5 to 1.5 mm M/L from the eye corner, and 0.8 to 0.5 mm in the Z direction. These injection coordinates are located within the visual cortex or the posterior somatosensory cortex in mice aged P3–P7. After the injections were completed, the transplanted mice were placed on a warm surface to recover from hypothermia. The mice were then returned to their mothers. Transplantation of cells involving the *Pcdhy*<sup>CAKO/CAKO</sup> alleles was performed utilizing cells from MGEs that had been cryopreserved (54).

**Tissue dissection and cell dissociation.** MGEs were dissected from E12.5 to E15.5 embryos as previously described (11). Dissections were performed in ice-cold L15 medium, and the dissected MGEs were kept in this medium at 4 °C. After collecting and genotyping the embryos, MGEs with the same genotype were pulled together and mechanically dissociated into a single-cell suspension by repeated pipetting in L15 medium containing DNase I (180  $\mu$ g/mL) using a P1000 pipette. For experiments involving cells from cryopreserved MGEs, cryovials were removed from –80 °C, thawed at 37 °C for 5 min, and the content of each tube was resuspended in a 15 mL falcon tube containing L15 medium at room temperature. The MGEs were washed twice with L15 to remove residual DMSO and dissociated as above.

**Cryopreservation of MGE in toto.** Dissected MGEs from each embryo were collected in 500  $\mu$ L L15 medium and kept on ice until cryopreserved. MGEs were resuspended in 10% DMSO in L15 medium and cryopreserved as previously described (54). Vials were cooled to –80 °C at a rate of –1 °C/min in a Nalgene™ Mr. Frosty Freezing Container and transferred the next day to liquid nitrogen for long-term storage. Importantly, tissue for genotyping was collected from each embryo and labeled with a code name matching the codename of each cryotube used for the cryopreservation.

**Cell counting.** GFP-positive cells and tdTomato-positive cells were counted in all layers of the neocortex. The vast majority of cells transplanted from the E13.5 MGE exhibited neuronal morphologies in the recipient's brain. Most cells migrated away from the injection site, but few astroglial cells remained at the injection site; these non-neuronal cells were not counted. Similarly, cells that migrated outside the cortex (typically into the hippocampus and striatum) were not included in the quantification. Images of cotransplanted cells were acquired on a SP8 (Leica) confocal microscope with a 10X magnification. Similarly, images of transplanted cells infected with lentivirus expressing *Pcdhy*C4-GFP were acquired on an SP8 confocal with a 10X magnification and a 2X digital zoom. GFP and tdTomato-positive cells were counted using Neurolucida (MBF). For all experiments, transplanted cells were counted from coronal sections along the rostral–caudal axis of the visual and somatosensory cortex and in at least 10 sections per animal; only sections containing more than 10 cells per condition were used. Data are presented as the fraction of transplant-derived cells that express GFP and/or tdTomato. The fraction of GFP/tdTomato cells does not reflect the absolute number of cells, but their relative contribution to the overall population of transplant-derived cells at each timepoint. We noted some variations in the initial proportions of tdTomato and ZsGreen cells at 6 DAT that are due to variations in dissection, dissociation, or cell damage. We used the 6 DAT data points as a baseline for comparison to 21 DAT. We analyzed the proportion of tdTomato and ZsGreen cells at 4 DAT and found very similar proportions to those observed at 6 DAT, indicating that the proportion at 6 DAT was a reliable baseline to determine differences in cIN survival between genotypes.

For experiments involving the expression of lentiviral-driven GFP or *Pcdhy* in transplanted cINs, survival was determined by comparing the fraction of infected

(tdTomato<sup>+</sup>GFP<sup>+</sup>) cells to the fraction of noninfected cells (tdTomato<sup>+</sup>GFP<sup>–</sup>) from the total number of transplanted cells (tdTomato<sup>+</sup>) in each brain section.

**Viral vector subcloning.** All lentiviral plasmids were cloned from the backbone construct pLenti-CAG-ires-EGFP (Addgene plasmid #122953). A Kozak sequence was added at the start of the coding region for all genes cloned. Plasmids were cloned using the Gibson Cloning Kit (NEB). The pLenti-CAG-EGFP construct was cloned by removing the ires sequence in between the BstXI and BamHI restriction sites from the backbone construct. To clone the pLenti-CAG-*Pcdhy*C4-EGFP (fusion construct), the pLenti-CAG-ires-EGFP plasmid was digested with BamHI and BstXI to remove the IRES sequence. A PCR generated *Pcdhy*C4 coding sequence lacking the stop codon and containing a two amino acid (Ser, Arg) linker was cloned upstream of the GFP coding sequence. This construct was used to express *Pcdhy*C4 fused to GFP.

**Viruses.** All lentiviruses used in this study were made in the laboratory. Briefly, viruses were produced in Lenti-X 293 T cells (Takara Bio). Cells were grown to  $\geq$ 90% confluency in maintenance media (DMEM/F-12, 15 mM HEPES, 2.5 mM GlutaMAX, 1% Pen/Strep, and 10% FBS) in 15-cm plates coated with Poly-D-lysine (Sigma-Aldrich P7405) at a final concentration of 0.1 mg per mL. Once cells reached the desired confluency, the media were changed to DMEM/F-12 + 2% FBS. Cells were transfected using TransIT<sup>®</sup>-293 Transfection Reagent (Mirusbio) and Opti-MEM (ThermoFisher). After 6 to 12 h posttransfection, the media were changed to lentivirus production media (DMEM/F-12, 15 mM HEPES, 2.5 mM GlutaMAX, 1% Pen/Strep, and 2% FBS), and 60  $\mu$ L of ViralBoost Reagent was added (ALSTEM) per 15-cm plate. Virus supernatant was collected 48 h posttransfection, filtered through a 45- $\mu$ m filter, and precipitated with Lentivirus Precipitation Solution (ALSTEM) overnight following the manufacturer's instructions. The viral pellet from two 15-cm plates was concentrated in a final volume of 100  $\mu$ L for *Pcdh* constructs and 200  $\mu$ L for the control construct.

**Viral infection of MGE precursor cells.** Following the dissociation of the MGEs, cells were concentrated by spinning in a table centrifuge for 5 min at 800g. The cell pellet was subsequently resuspended in an equal volume of lentivirus and L15 medium. The cell-virus mix was incubated at 22 to 32 °C at 1,000 rpm (190 rcf) for 3 h, mixing every 30 min.

**Western blot analysis.** Protein lysates were generated from infected and non-infected neuronal cultures. Protein lysates were loaded into Bolt™ Bis-Tris Plus Mini Protein Gels, 4 to 12%, 1.0 mm, WedgeWell™ precast gels (Invitrogen). Protein lysates of uniform volumes were used for all experimental conditions, except for the GFP lentivirus condition, which was diluted 1:2 in lysis buffer, due to a higher rate of infection. Protein samples were separated via SDS/PAGE and transferred onto nitrocellulose membranes using the XCell SureLock Mini-Cell Electrophoresis System (Invitrogen). After protein transfer, membranes were blocked in 5% nonfat milk in Tris-buffered Saline with 0.1% Tween 20 (TBST) for at least 1 h. Membranes were then washed three times for 5 min in TBST. An anti-GFP antibody (Invitrogen. 1:500 RRID: AB\_2307355) was diluted in 5% TBST, and membranes were incubated overnight at 4 °C. Blots were once again washed three times for 5 min. The membrane was then incubated for at least 1 h in horseradish peroxidase (HRP)-conjugated secondary antibody (Invitrogen, 1:5,000 RRID: AB\_228338) diluted into 5% nonfat milk in TBST. Signals were detected using SuperSignal West Pico Enhanced Chemiluminescent Substrates (Thermo Fisher Scientific) on a LI-COR Odyssey FC imager.

**Immunostaining.** P21 and older mice were fixed by transcardiac perfusion with 10 mL of PBS followed by 10 mL of 4% formaldehyde/PBS solution (both at 4 °C); transcardiac perfusion of 5 mL of either solution was used for P15 and younger mice. After perfusion, brains were incubated overnight in 4% formaldehyde/PBS solution (12 to 24 h) at 4 °C, then rinsed with PBS and cryoprotected in 30% sucrose/PBS solution for 48 h at 4 °C. Unless otherwise stated, immunohistochemistry was performed on 30- $\mu$ m floating sections in Tris Buffered Saline (TBS) solution containing 10% normal donkey serum and 0.5% Triton X-100 for all procedures on postnatal mice. All washing steps were done in 0.1% Triton X-100 TBS for all procedures. Sections were incubated overnight at 4 °C with selected antibodies, followed by incubation at 4 °C overnight in donkey secondary antibodies (Jackson ImmunoResearch Laboratories). Brain sections that had been transplanted with lentivirus-infected MGE cells were incubated for 2 d in primary antibodies and overnight with secondary antibodies to enhance the virally expressed reporter GFP. For cell counting and post hoc examination

of marker expression, sections were stained using chicken anti-GFP (1:2500, Aves Labs, GFP-1020, RRID: AB\_10000240), rabbit anti-RFP (Rockland), and rat anti-tdTomato (Kerafast). For staining against *PcdhyC5*, *Cux1*, *Ctip2*, *PV*, *SST*, and *ZsGreen* (SI Appendix, Fig. S1) brains were cryosectioned at 12  $\mu\text{m}$  thickness, dried directly onto microscope slides, and washed 3X for 5 min in 1X TBS. Sections were then incubated in a blocking solution (2.5% BSA, 0.5% TritonX, in 1X TBS) for 2 h at room temperature and then washed 3X for 5 min. The primary antibodies were diluted in a solution of 2.5% BSA, 0.25% TritonX in TBS, and then applied to sections overnight at 4 °C. Sections were then washed 3X for 5 min in 1X TBS before being incubated with host-appropriate secondaries for 2 h at room temperature at a 1:500 dilution in 2.5% BSA 0.25% TritonX in TBS. The primary antibodies used in this experiment were as follows: *PcdhyC5* (Invitrogen, 1:150, RRID: AB\_2724958), *Ctip2* (Abcam, 1:200, RRID: AB\_2064130), *Cux1* (Santa Cruz Biotechnology, 1:100 RRID: AB\_2261231), *PV* (Swant, 1:1000, RRID: AB\_2631173), *SST* (Sigma, 1:100, RRID: AB\_2255365), and *ZsGreen* (Nissin Medical, 1:200 MSFR106440). Multiple dilutions of five different *PCDH4* antibodies were tested, but none worked for immunostaining: (Neuromab, 1:500-50, RRID: AB\_2877443), (Thermo Fisher Scientific, 1:50-500, RRID: AB\_2548856), (Novus, 1:50-500, RRID: AB\_11015449), (ABR, 1:50-500, Rabbit A337005), and (ABR, 1:50-500, Chicken).

***PcdhyC5* protein quantification.** Quantifications were completed using FIJI. The mean signal intensity was acquired from each cell using the FIJI ROI manager tool. The mean signal intensity measurements were normalized over the background signal levels (intersomatic spaces). Cells were considered positive when the mean intensity was above the background measurements.

**RNAscope.** Brains of *Nkx2.1<sup>Cre</sup>*, *Ai6* animals at P5, P7, and P14 were fixed, postfixed, and cryoprotected (as described in *Immunostaining*). Brains were cryosectioned and mounted directly onto microscope slides before being stored at  $-80^{\circ}\text{C}$ . The RNA scope experiments were completed as per the manufacturer's instructions (RNAscope multiplex fluorescent reagent kit v2, Advanced Cell Diagnostics, Inc.). Sections were equilibrated by a 10-min incubation at  $-20^{\circ}\text{C}$  followed by 10 min incubation at room temperature. Brain sections were dehydrated using increasing concentrations of ethanol (50%, 70%, and 100%) for 5 min incubations at room temperature. Sections were then incubated with RNAscope Hydrogen Peroxide solution for 10 min at room temperature, before four washes in distilled water. To perform the target retrieval step of the protocol, slides were incubated in distilled water for 10 s and then RNAscope 1X target retrieval buffer for 15 min using an Oyster brand steamer at  $\sim 99^{\circ}\text{C}$ . Sections were then washed for 15 s in distilled water before being transferred to 100% ethanol for 3 min at room temperature. Slides were then dried in an incubator at  $60^{\circ}\text{C}$  for 5 min. To reduce reagent usage, a hydrophobic barrier pen was used to surround the tissue. Tissue was incubated in  $\sim 5$  drops of RNAscope Protease III and incubated at  $40^{\circ}\text{C}$  for 30 min using a HybEZ Humidity Control Tray in a HybEZ oven.

Tissue was then incubated in the *PcdhyC4* (probe 835791-C3) and *PcdhyC5* (probe 850581) probes for 2 h at  $40^{\circ}\text{C}$ . After incubation, probes were hybridized with AMP1, AMP2, and AMP3 (in that order) through individual incubations at  $40^{\circ}\text{C}$  for 30 min (AMP3 incubation 15 min incubation). Our probes were Channel-1 (*PcdhyC5*) and Channel-3 (*PcdhyC4*), so we skipped the development HRP-C2 signal and continued directly to the development of the HRP-C3 RNAscope Multiplex FL v2 HRP-C2. Tissue was incubated with 3 to 4 drops of

RNAscope multiplex v2 HRP-C3 solution for 15 min at  $40^{\circ}\text{C}$ , followed by a 2 min wash in 1X RNA scope wash buffer. Then, tissue was incubated with Cy3 (Thermo Fisher Scientific, 1:1000) diluted in TSA buffer (Advanced Cell Diagnostics, Inc.), followed by another 2-min wash in 1X Wash Buffer. This process was completed again using the RNAscope multiplex v2 HRP-C3 solution and Cy5 (Thermo Fisher Scientific, 1:1000). Slides were washed 3X in distilled water for 5 min, before being mounted using Fluoromount-G, DAPI mounting media.

**Quantification of RNAscope probes.** Quantifications of the *PcdhyC4* and *PcdhyC5* transcripts in the RNAscope experiments were completed by measuring the mean signal intensity of both *PcdhyC4* and *PcdhyC5* probes over the cell area using FIJI. Cells with minimal *PcdhyC4* or *PcdhyC5* signals were used to set a lower mean intensity threshold. Cells with a signal intensity value higher than the mean intensity threshold were considered positive for *PcdhyC4* and *PcdhyC5*.

**Analysis of previously published single-cell RNA sequencing datasets.** Data from Tasic et al. (38), were obtained via the Broad Institute Single Cell Portal ([https://singlecell.broadinstitute.org/single\\_cell/study/SCP6/a-transcriptomic-taxonomy-of-adult-mouse-visual-cortex-visp](https://singlecell.broadinstitute.org/single_cell/study/SCP6/a-transcriptomic-taxonomy-of-adult-mouse-visual-cortex-visp)). Cells were grouped by GABAergic vs glutamatergic designation or cluster type, as determined by the data generators. RPKM values for each cell in each cluster type were averaged and plotted using PRISM. Data obtained from Yao et al. (37), were obtained from the UCSC Cell Browser (<https://cells.ucsc.edu/?ds=allen-celltypes+mouse-cortex+mouse-cortex-2019>). Cells were grouped based on either GABAergic or glutamatergic designations or by cluster type determined by the data generators. Absolute transcript values for each cell in each cluster type were averaged and plotted using PRISM.

**Statistical analysis.** Quantifications for transplantation experiments were performed by two different people, one of whom was blinded to the genotype. Average mutant and WT survival ratios in each mouse were estimated by counting the transplanted mutant and wild-type cells in each of  $\sim 10$  sections. We used an ANOVA to determine whether the survival ratios in 6 DAT mice were significantly different from those in 21 DAT mice.

**Data, Materials, and Software Availability.** All study data are included in the article and/or SI Appendix. Previously published data were used for this work (37, 38).

**ACKNOWLEDGMENTS.** This work was supported by NIH Grant R01MH122478 to A.A.-B., A.R.H., and M.P.S.; NIH Grants R01 NS028478 and R01 EY02517; and a generous gift from the John G. Bowes Research Fund to A.A.-B.; NIH Grants R01 NS055272 and R21 NS090030 to J.A.W.; NIH Grants R01NS116598; Hearing Research Inc.; the PBR Breakthrough Fund; and the Coleman Memorial Fund to A.R.H.; A.A.-B. is the Heather and Melanie Muss Endowed Chair and Professor of Neurological Surgery at UCSF. M.P.S. is a recipient of the Research to Prevent Blindness Disney Award for Amblyopia Research.

Author affiliations: <sup>a</sup>Department of Neurological Surgery and The Eli and Edythe Broad Center of Regeneration Medicine and Stem Cell Research, University of California, San Francisco, San Francisco, CA 94143; <sup>b</sup>Department of Biology, The University of Iowa, Iowa City, IA 52242; <sup>c</sup>Department of Physiology, University of California, San Francisco, San Francisco, CA 94143; <sup>d</sup>Department of Otolaryngology-Head and Neck Surgery, University of California, San Francisco, San Francisco, CA 94143; and <sup>e</sup>Kavli Institute for Fundamental Neuroscience, University of California, San Francisco, San Francisco, CA 94143

- C. Y. Kuan, K. A. Roth, R. A. Flavell, P. Rakic, Mechanisms of programmed cell death in the developing brain. *Trends Neurosci.* **23**, 291-297 (2000).
- R. W. Oppenheim, Cell death during development of the nervous system. *Annu. Rev. Neurosci.* **14**, 453-501 (1991).
- E. J. Huang, L. F. Reichardt, Neurotrophins: Roles in neuronal development and function. *Annu. Rev. Neurosci.* **24**, 677-736 (2001).
- L. Aloe, G. N. Chaldakov, The multiple life of nerve growth factor: Tribute to Rita Levi-Montalcini (1909-2012). *Balkan Med. J.* **30**, 4-7 (2013).
- Y. Yamaguchi, M. Miura, Programmed cell death in neurodevelopment. *Dev. Cell* **32**, 478-490 (2015).
- R. Levi-Montalcini, The nerve growth factor 35 years later. *Science* **237**, 1154-1162 (1987).
- Y. Yamaguchi, M. Miura, Programmed cell death in neurodevelopment. *Dev. Cell* **32**, 478-490 (2015).
- S. Rauskolb et al., Global deprivation of brain-derived neurotrophic factor in the CNS reveals an area-specific requirement for dendritic growth. *J. Neurosci.* **30**, 1739-1749 (2010).
- I. Silos-Santiago, A. M. Fagan, M. Garber, B. Fritsch, M. Barbacid, Severe sensory deficits but normal CNS development in newborn mice lacking TrkB and TrkC tyrosine protein kinase receptors. *Eur. J. Neurosci.* **9**, 2045-2056 (1997).
- V. Nikoletopoulou et al., Neurotrophin receptors TrkA and TrkC cause neuronal death whereas TrkB does not. *Nature* **467**, 59-63 (2010).
- D. G. Southwell et al., Intrinsically determined cell death of developing cortical interneurons. *Nature* **491**, 109-113 (2012).
- J. L. R. Rubenstein, M. M. Merzenich, Model of autism: Increased ratio of excitation/inhibition in key neural systems. *Genes Brain Behav.* **2**, 255-267 (2003).
- D. A. Lewis, T. Hashimoto, D. W. Volk, Cortical inhibitory neurons and schizophrenia. *Nat. Rev. Neurosci.* **6**, 312-324 (2005).
- H.-T. Chao et al., Dysfunction in GABA signalling mediates autism-like stereotypies and Rett syndrome phenotypes. *Nature* **468**, 263-269 (2010).
- O. Marin, Interneuron dysfunction in psychiatric disorders. *Nat. Rev. Neurosci.* **13**, 107-120 (2012).
- L. Verret et al., Inhibitory interneuron deficit links altered network activity and cognitive dysfunction in Alzheimer model. *Cell* **149**, 708-721 (2012).
- E. Rossignol, Genetics and function of neocortical GABAergic interneurons in neurodevelopmental disorders. *Neural Plast.* **2011**, 649325 (2011).
- F. K. Wong et al., Pyramidal cell regulation of interneuron survival sculpts cortical networks. *Nature* **557**, 668-673 (2018).



19. L. Seress, M. Frotscher, C. E. Ribak, Local circuit neurons in both the dentate gyrus and Ammon's horn establish synaptic connections with principal neurons in five day old rats: A morphological basis for inhibition in early development. *Exp. Brain Res.* **78**, 1–9 (1989).
20. J.-M. Yang, J. Zhang, Y.-Q. Yu, S. Duan, X.-M. Li, Postnatal development of 2 microcircuits involving fast-spiking interneurons in the mouse prefrontal cortex. *Cereb. Cortex* **24**, 98–109 (2012).
21. B. W. Connors, L. S. Benardo, D. A. Prince, Coupling between neurons of the developing rat neocortex. *J. Neurosci.* **3**, 773–782 (1983).
22. R. Tyzio *et al.*, The establishment of GABAergic and glutamatergic synapses on CA1 pyramidal neurons is sequential and correlates with the development of the apical dendrite. *J. Neurosci.* **19**, 10372–10382 (1999).
23. Y. Ben-Ari, I. Khalilov, A. Represa, H. Gozlan, Interneurons set the tune of developing networks. *Trends Neurosci.* **27**, 422–427 (2004).
24. R. Priya *et al.*, Activity regulates cell death within cortical interneurons through a calcineurin-dependent mechanism. *Cell Rep.* **22**, 1695–1709 (2018).
25. Z. R. S. Duan *et al.*, GABAergic restriction of network dynamics regulates interneuron survival in the developing cortex. *Neuron* **105**, 75–92.e5 (2020).
26. Q. Wu, T. Maniatis, A striking organization of a large family of human neural cadherin-like cell adhesion genes. *Cell* **97**, 779–790 (1999).
27. Q. Wu *et al.*, Comparative DNA sequence analysis of mouse and human protocadherin gene clusters. *Genome Res.* **11**, 389–404 (2001).
28. M. J. Molumby, A. B. Keeler, J. A. Weiner, Homophilic protocadherin cell–cell interactions promote dendrite complexity. *Cell Rep.* **15**, 1037–1050 (2016).
29. S. Katori *et al.*, Protocadherin- $\alpha$ 2 is required for diffuse projections of serotonergic axons. *Sci. Rep.* **7**, 15908 (2017).
30. G. Mountoufaris *et al.*, Multicenter Pcdh diversity is required for mouse olfactory neural circuit assembly. *Science* **356**, 411–414 (2017).
31. A. M. Garrett, D. Schreiner, M. A. Lobas, J. A. Weiner,  $\gamma$ -protocadherins control cortical dendrite arborization by regulating the activity of a FAK/PKC/MARCKS signaling pathway. *Neuron* **74**, 269–276 (2012).
32. W. V. Chen, T. Maniatis, Clustered protocadherins. *Development* **140**, 3297 (2013).
33. W. R. Mancia Leon *et al.*, Clustered gamma-protocadherins regulate cortical interneuron programmed cell death. *eLife* **9**, e55374 (2020).
34. J. A. Weiner, X. Wang, J. C. Tapia, J. R. Sanes, Gamma protocadherins are required for synaptic development in the spinal cord. *Proc. Natl. Acad. Sci. U.S.A.* **102**, 8–14 (2005).
35. J. L. Lefebvre, Y. Zhang, M. Meister, X. Wang, J. R. Sanes, gamma-Protocadherins regulate neuronal survival but are dispensable for circuit formation in retina. *Development* **135**, 4141–4151 (2008).
36. A. M. Garrett *et al.*, CRISPR/Cas9 interrogation of the mouse Pcdhg gene cluster reveals a crucial isoform-specific role for Pcdhg4. *PLoS Genet.* **15**, e1008554 (2019).
37. Z. Yao *et al.*, A taxonomy of transcriptomic cell types across the isocortex and hippocampal formation. *Cell* **184**, 3222–3241.e26 (2021).
38. B. Tasic *et al.*, Shared and distinct transcriptomic cell types across neocortical areas. *Nature* **563**, 72–78 (2018).
39. D. M. Steffen *et al.*, A unique role for Protocadherin  $\gamma$ C3 in promoting dendrite arborization through an Axin1-dependent mechanism. *J. Neurosci.* **43**, 918–935 (2023), <https://doi.org/10.1523/JNEUROSCI.0729-22.2022>.
40. L. Madisen *et al.*, A robust and high-throughput Cre reporting and characterization system for the whole mouse brain. *Nat. Neurosci.* **13**, 133–140 (2010).
41. W. V. Chen *et al.*, Functional significance of isoform diversification in the protocadherin gamma gene cluster. *Neuron* **75**, 402–409 (2012).
42. X. Wang *et al.*, Gamma protocadherins are required for survival of spinal interneurons. *Neuron* **36**, 843–854 (2002).
43. T. Prasad, X. Wang, P. A. Gray, J. A. Weiner, A differential developmental pattern of spinal interneuron apoptosis during synaptogenesis: Insights from genetic analyses of the protocadherin- $\gamma$  gene cluster. *Development* **135**, 4153–4164 (2008).
44. C. H. Carriere *et al.*, The  $\gamma$ -protocadherins regulate the survival of GABAergic interneurons during developmental cell death. *J. Neurosci.* **40**, 8652–8668 (2020).
45. H. Kobayashi *et al.*, Isoform requirement of clustered protocadherin for preventing neuronal apoptosis and neonatal lethality. *iScience* **26**, 105766 (2023).
46. C. A. Thu *et al.*, Generation of single cell identity by homophilic interactions between combinations of  $\alpha$ ,  $\beta$  and  $\gamma$  protocadherins. *Cell* **158**, 1045 (2014).
47. K. M. Goodman *et al.*, How clustered protocadherin binding specificity is tuned for neuronal self-/nonself-recognition. *eLife* **11**, e72416 (2022).
48. F. K. Wong *et al.*, Serotonergic regulation of bipolar cell survival in the developing cerebral cortex. *Cell Rep.* **40**, 111037 (2022).
49. R. R. Buss, W. Sun, R. W. Oppenheim, Adaptive roles of programmed cell death during nervous system development. *Annu. Rev. Neurosci.* **29**, 1–35 (2006).
50. D. Purves, J. Lichtman, Trophic effects of targets on neurons in *Principles of neural development*, J. Simpson, Ed. (Sunderland, Sinauer Associates Inc, 1985), chap. 7, pp. 155–178.
51. M. Iqbal *et al.*, Biallelic variants in PCDHGC4 cause a novel neurodevelopmental syndrome with progressive microcephaly, seizures, and joint anomalies. *Genet. Med.* **23**, 2138–2149 (2021).
52. H. Wichterle, J. M. Garcia-Verdugo, D. G. Herrera, A. Alvarez-Buylla, Young neurons from medial ganglionic eminence disperse in adult and embryonic brain. *Nat. Neurosci.* **2**, 461–466 (1999).
53. F. T. Merkle, Z. Mirzadeh, A. Alvarez-Buylla, Mosaic organization of neural stem cells in the adult brain. *Science* **317**, 381–384 (2007).
54. D. Rodríguez-Martínez, M. M. Martínez-Losa, M. Alvarez-Dolado, Cryopreservation of GABAergic neuronal precursors for cell-based therapy. *PLoS ONE* **12**, e0170776 (2017).